
Sn⁴⁺ Precursor Enables 12.4% Efficient Kesterite Solar Cell from DMSO Solution with Open Circuit Voltage Deficit Below 0.30 V

Yuancai Gong¹, Yifan Zhang¹, Erin Jedlicka², Rajiv Giridharagopal², James A. Clark³, Weibo Yan¹, Chuanyou Niu¹, Ruichan Qiu¹, Jingjing Jiang¹, Shaotang Yu¹, Sanping Wu¹, Hugh W. Hillhouse³, David S. Ginger², Wei Huang¹, and Hao Xin^{1*}

ABSTRACT. The limiting factor preventing kesterite (CZTSSe) thin film solar cell performance further improvement is the large open-circuit voltage deficit ($V_{oc,def}$) issue, which is 0.345V for the current world record device with an efficiency of 12.6%. In this work, SnCl₄ and SnCl₂·2H₂O are respectively used as tin precursor to investigate the $V_{oc,def}$ issue of dimethyl sulfoxide (DMSO) solution processed CZTSSe solar cells. Different complexations of tin compounds with thiourea and DMSO lead to different reaction pathways from solution to absorber material and thus dramatic difference in photovoltaic performance. The coordination of Sn²⁺ with Tu leads to the formation of SnS and ZnS and Cu₂S in the precursor film, which converted to selenides first and then fused to CZTSSe, resulting in poor film quality and device performance. The highest efficiency obtained from this film is 8.84% with a $V_{oc,def}$ of 0.391V. The coordination of Sn⁴⁺ with DMSO facilitates direct formation of kesterite CZTS phase in the precursor film which directed converted to CZTSSe during selenization, resulting in compositional uniform absorber and high device performance. A device with active area efficiency 12.2% and a $V_{oc,def}$ of 0.344 V was achieved from Sn⁴⁺ solution processed absorber. Furthermore, CZTSSe/CdS heterojunction heat treatment (JHT) significantly improved Sn⁴⁺ device performance but had slightly negative effect on Sn²⁺ device. A champion CZTSSe solar cell with a total area efficiency of 12.4% (active area efficiency 13.6%) and low $V_{oc,def}$ of 0.297 V was achieved from Sn⁴⁺ solution. Our results demonstrate the preformed uniform kesterite phase enabled by Sn⁴⁺ precursor is the key in achieving highly efficient kesterite absorber material. The lowest $V_{oc,def}$ and high efficiency achieved here shines new light on the future of kesterite solar cell.

Keywords: kesterite solar cell, V_{oc} deficit, SnCl₄, reaction pathway, heterojunction heat treatment

INTRODUCTION

Kesterite Cu₂ZnSn(S,Se)₄ (CZTSSe) semiconductors have great potential as low cost photovoltaic absorber

materials[1-7] because they have theoretically high efficiency to similar structured copper indium gallium selenides (Cu(In,Ga)Se₂, CIGS) but composed of less-toxic and earth-abundant elements. However, the efficiency of CZTSSe solar cell is only 12.6%[8, 9] whereas the efficiency of CIGS solar cell has recently reached 23.35%.[10] The barrier for CZTSSe efficiency further improvement is the large open-circuit voltage deficit ($V_{oc,def} = V_{oc}^{SQ} - V_{oc}$, V_{oc}^{SQ} is the maximum achievable V_{oc} based on Shockley-Queisser limit[11]) which is above 0.34 V for CZTS but below 0.15 V for CIGS solar cells. Possible reasons for the large $V_{oc,def}$ include potential and band gap fluctuations,[12] deep defects,[13] recombination at interfaces,[14, 15] and secondary phases.[16] Improving V_{oc} is a must for practical application of kesterite solar cells.[17, 18] Recent efforts in addressing the $V_{oc,def}$ issue are mainly focused on extrinsic doping[2, 19] or alloying[3, 11, 20, 21]. However, none of the reported doping or alloying strategies has led to efficiency higher than current world record, indicating the optoelectronic properties of kesterite absorbers are more likely governed by the intrinsic defects.[6, 22]

The absorber materials of chalcogenide (CIGS and CZTSSe) thin film solar cells are fabricated from vacuum[4, 10, 23] or solution[24-28] deposited precursor films by reacting with S, H₂S, Se, H₂Se or a mixture of them (so called sulfurization and selenization) to facilitate grain growth. The property of the absorber material and the photovoltaic performance of the solar cells highly depends on the composition of the precursor film and the reaction pathway from the precursor to the absorber.[9, 21] This should be more significant for kesterite because it has two metal elements (Cu and Sn) that have variable oxidation state and Sn related deep defects have been reported to be detrimental to photovoltaic performance.[13, 29, 30] Thus, investigation on how Sn precursor oxidation state affects the reaction path from precursor film to absorber material and

¹Key Laboratory for Organic Electronics and Information Displays & Jiangsu Key Laboratory for Biosensors, Institute of Advanced Materials (IAM), Jiangsu National Synergetic Innovation Center for Advanced Materials (SICAM), Nanjing University of Posts & Telecommunications, 9 Wenyuan Road, Nanjing 210023, China.

²Department of Chemistry, University of Washington, Seattle, WA, 98195 USA

³Department of Chemical Engineering, University of Washington, Seattle, WA, 98195 USA

* Corresponding author (jambxin@njupt.edu.cn)

photovoltaic performance might be able to provide new insight of kesterite. Surprisingly, to the best of our knowledge, no such study has been performed. Compared to vacuum based approaches, which mostly use metal[9, 23] or stannous sulfide[4] as Sn precursor, solution based method provides an excellent platform for this investigation because the oxidation states of Sn can be precisely controlled by using stannous (II) or stannic (IV) salts as Sn precursor.

Some of the authors had previously reported 4.1% efficient CZTSSe solar cells with the absorber fabricated from DMSO solution using $\text{SnCl}_2 \cdot 2\text{H}_2\text{O}$, $\text{Cu}(\text{OAc})_2$, ZnCl_2 , and thiourea (Tu) as precursors.[31] Later, by facilitating complete redox reaction between $\text{SnCl}_2 \cdot 2\text{H}_2\text{O}$ and $\text{Cu}(\text{OAc})_2$ ($2\text{Cu}^{2+} + \text{Sn}^{2+} = 2\text{Cu}^{+} + \text{Sn}^{4+}$) the efficiency of CZTSSe solar cell was improved to 8.3%.[25] Although the redox reaction was intentionally to reduce detrimental Cu^{2+} , more Sn^{2+} was oxidized to Sn^{4+} , which may also account for the improved performance. The efficiency of DMSO solution based CZTSSe solar cell was further improved to beyond 11% by alkali metal ions along with fabrication condition optimization.[2, 19, 32] In the above DMSO solutions, Sn and Cu precursors were both in +2 oxidation states (SnCl_2 , CuCl_2 or $\text{Cu}(\text{OAc})_2$), even with complete redox reaction between Sn^{2+} and Cu^{2+} , there was still Sn^{2+} in the solution due to the requirement of a copper poor ($\text{Cu}:\text{Sn} < 2$) kesterite composition for better device performance. This means at least two reaction paths (Sn^{2+} and Sn^{4+}) were involved in converting the precursors from solution to the absorber materials.

To investigate the reaction paths of Sn^{2+} and Sn^{4+} and their effect on kesterite photovoltaic performance, in this report, we have respectively used $\text{SnCl}_2 \cdot 2\text{H}_2\text{O}$ and SnCl_4 as tin source and CuCl as copper source (to avoid redox reaction) to make Sn^{2+} and Sn^{4+} precursor solution and fabricate CZTSSe solar cells. We found that the two solutions indeed took different reaction pathways from solution to absorber film, which resulted in dramatic difference in photovoltaic performance. A high crystalline precursor film composed of multiple phases including SnS was formed from Sn^{2+} solution whereas uniform amorphous kesterite phase without secondary phases was obtained from Sn^{4+} solution. Although both precursor films converted to high crystalline absorbers upon selenization, the different reaction pathway leads to dramatic difference in film morphology, composition and photovoltaic properties. A maximum active area efficiency of 12.2% with $V_{\text{oc,def}}$ of 0.344 V was obtained from Sn^{4+} device, which was only 8.84% with $V_{\text{oc,def}}$ of 0.391 V for Sn^{2+} device. Furthermore, heterojunction heat treatment (JHT) of CZTSSe/CdS significantly improved Sn^{4+} device performance but had slightly negative effect on Sn^{2+} device. A champion CZTSSe solar cell with a total area efficiency of 12.4% (active area efficiency of 13.6%) and record low $V_{\text{oc,def}}$ of 0.297 V was achieved from Sn^{4+} solution.

EXPERIMENTAL SECTION

Preparation of the molecular precursor solutions

The precursor solutions were prepared in a glovebox with controlled O_2 and H_2O level below 5 ppm at room temperature. First, CuCl -thiourea (Tu) solution was made by adding 1.602 g Tu (99%, Aladdin, recrystallized twice) to a vial containing 4 mL dimethyl sulfoxide (DMSO, 99.8%, J&K) under stirring until completely dissolved, then 0.582g CuCl (99.999%, Alfa) was added to make a clear solution. For Sn^{2+} precursor solution, 0.903g $\text{SnCl}_2 \cdot 2\text{H}_2\text{O}$ (99.99%, Aladdin), 0.567g ZnCl_2 (99.95%, Aladdin) and 3 mL DMSO were subsequently added to the above CuCl -Tu DMSO solution and stirred until completely dissolved. For the Sn^{4+} solution, 1.042 g of SnCl_4 (99.99%, Alfa) was added into a second vial, the vial was sealed to prevent SnCl_4 evaporation. Then, 3 mL DMSO was injected into the vial by a syringe. SnCl_4 reacts with DMSO violently and forms white precipitate. Then 0.763 g $\text{Zn}(\text{OAc})_2$ (99.99%, Aladdin) was added to the SnCl_4 -DMSO suspension and stirred until a clear solution was formed. This solution was then mixed with CuCl -Tu solution to yield a pale yellow solution. We use $\text{Zn}(\text{OAc})_2$ instead of ZnCl_2 as Zn source for Sn^{4+} precursor solution because SnCl_4 coordinates with DMSO and forms $\text{Sn}(\text{DMSO})_4\text{Cl}_4$ (Figure S6), which has low solubility in DMSO. The use of $\text{Zn}(\text{OAc})_2$ reduces Cl^- concentration and stabilize the precursor solution.

Fabrication of CZTSSe absorber films

Molybdenum-coated soda-lime glass (MSLG) substrates were cleaned by sequential sonication in acetone and 2-propanol, each for 15 min, and dried under N_2 flow. The precursor film fabrication was done in a glovebox with O_2 and H_2O level below 5 ppm. The CZTS precursor solution was filtered with 0.8 μm PTFE filter and spin-coated on the clean MSLG substrate at 1500 rpm for 60s. The wet film was immediately annealed on a hot plate at 420°C for 2 min. The coating-annealing-cooling cycle was repeated seven times to build up a precursor film with a thickness $\sim 2 \mu\text{m}$. The film was then put into a graphite box with Se tablets ($\sim 500 \text{ mg}$) and placed in Rapid Heating furnace tube for selenization. The selenization was performed at 550°C for 20 min with Ar flow rate of 20 sccm.

Fabrication of solar cell devices

The cadmium sulfide buffer layer of thickness 40~50 nm was deposited by the chemical bath deposition (CBD) method.[27] For samples without junction heat treatment (JHT), a window layer containing 50 nm i-ZnO and 250 nm ITO was directly deposited on top of CdS by RF sputtering at room temperature. For heterojunction heat treatment, the samples (MSLG/CZTSSe/CdS) were loaded on sample holder and put into the chamber for sputtering; the chamber was pumped down to vacuum below $2 \times 10^{-3} \text{ Pa}$. The sample holder (and samples) was heated to 200°C within 30 min and kept at 200°C for a designed time (2 hours or 20 hours), then the window layer containing 50 nm i-ZnO and 150 nm ITO were deposited at 200°C right after the JHT. Finally, top contact grids of nickel (50 nm) and aluminum (200 nm) were fabricated in a separate thermal deposition system through a shadow mask. The solar cell area was defined by mechanical scribing for approximately 0.105 cm^2 and the accurate area

was individually measured as described in the Supporting Information. ITO sputtered at room temperature has higher resistance than that sputtered at 200°C due to poor crystallinity, so the ITO of samples without JHT is thicker (250 nm) than samples with JHT (150 nm) in order to have similar conductivity. The thinner ITO has slightly higher transparency than thicker ITO.

Film characterization

X-ray diffraction (XRD) spectra (2 θ scan) were collected by a Siemens D5005 X-ray powder diffraction system using Cu K ($\lambda = 1.5406 \text{ \AA}$) X-ray as the source. The Raman spectra were acquired on Renishaw in Via microscope using 532 or 785 nm Laser diode as the excitation source. The film surface morphology and elemental composition analysis were measured on Hitachi S4800 scanning electron microscope (SEM) using 5 kV power for imaging and 15 or 20 kV power for energy dispersive X-ray (EDX) spectroscopy. The film composition profile was acquired by glow discharge optical emission spectroscopy (GDOES) using a Horiba GD-Profilier 2 instrument with an anode of 4 mm. Plasma optimization and GDOES calibration were based on information presented by Payling and Nelis¹. Photoluminescence spectra were acquired on a modified Horiba LabRAM HR-800 using a 785 nm laser diode as excitation source and a liquid nitrogen cooled InGaAs array as detector.

Device characterization

The current density-voltage (J-V) curves were measured using Keithley 2400 Source Meter under simulated AM 1.5 sunlight at 100 mW/cm² irradiance generated by an AAA sun simulator (CROWNTech, Inc.) with the intensity calibrated by an NREL calibrated Si reference cell. The external quantum efficiency (EQE) of the solar cells was measured on Enlitech QE-R3018 using calibrated Si and Ge diodes (Enli technology Co. Ltd.) as references.

RESULTS AND DISCUSSION

Figure 1a and Figure 1b show the active area current density-voltage (J-V) and external quantum efficiency (EQE) curves of the best performing Sn²⁺ and Sn⁴⁺ devices fabricated under standard condition with 98 nm MgF₂ antireflective coating (ARC). The device structure and a representative cross-section SEM image of Sn⁴⁺ solar cell are shown in Figure 1c. Since our devices have relatively larger grids (~10.5% total area) than ideal condition (~4%) due to mask design and grid fabrication condition, we use active area efficiency to better reflect absorber property and total area efficiency for fair comparison with literature, both are specified throughout the report. The method of device total and active area calculation is given in Figure S1. A maximum active area power conversion efficiency (PCE) of 12.2% with J_{sc} , V_{oc} , FF of 37.2 mA/cm², 0.475 V and 68.8% was achieved from Sn⁴⁺ solution. The PCE, J_{sc} , V_{oc} , FF obtained from Sn²⁺ solution were respectively 8.84%, 35.5 mA/cm², 0.421 V and 59.1%. Sn⁴⁺ solar cells not only have higher value in all device parameters than Sn²⁺ solar cells but also exhibit much smaller scattering in all device parameters (Figure 1d and Table S1), revealing higher quality and uniformity of Sn⁴⁺ absorber. The photoluminescence spectra (Fig-

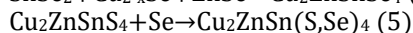
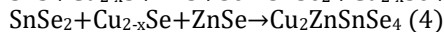
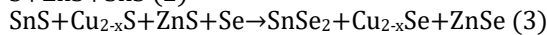
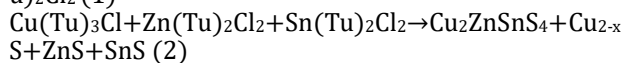
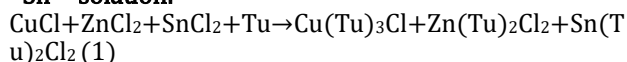
ure S2) show that Sn⁴⁺ absorber exhibits higher PL intensity, higher peak energy and narrower full width at the half maximum (FWHM) than Sn²⁺ film. The EQE spectra (Figure 1b) reveal Sn⁴⁺ device has better carrier collection efficiency than Sn²⁺ device, especially in the near infrared range. The bandgaps of the CZTSSe absorber materials estimated from the EQE data (Figure 1b, inset) are 1.050 eV for Sn²⁺ device and 1.058 eV for Sn⁴⁺ device. Based on V_{oc}^{SQ} calculated from equation $V_{oc}^{SQ} = 0.932 \times E_g - 0.167$, the $V_{oc,def}$ of Sn²⁺ and Sn⁴⁺ devices are calculated to be 0.391 V and 0.344 V, respectively. A $V_{oc,def}$ of 0.344 V is one of the lowest value achieved from kesterite without extra modification such as doping,[6, 22] grain boundary passivation,[33] or alloying,[6, 22] demonstrating the advance of Sn⁴⁺ precursor in achieving high quality kesterite absorber.

Figure 1e shows the powder X-ray diffraction (XRD) patterns of the precursor and absorber films fabricated parallel to the best performing devices in Figure 1a. For Sn²⁺ precursor film, sharp diffraction peaks that can be assigned to kesterite Cu₂ZnSnS₄ (PDF# 26-0575) and SnS (PDF#39-0354) are observed together with detectable peak from Cu_{2-x}S (Figure 1e). The formation of SnS and Cu_{2-x}S suggests the existence of ZnS because of the Zn-rich composition, although ZnS cannot be distinguished from CZTS due to diffraction peak overlap. The high crystallinity of Sn²⁺ precursor film is also confirmed by SEM (Figure 1f) and Raman (Figure S3). In contrast, Sn⁴⁺ precursor film only contains amorphous Cu₂ZnSnS₄ as revealed by XRD (Figure 1e) and Raman (Figure S3) results. Both precursor films converted to high crystalline absorber film upon selenization with different morphology (Figure 1f, and Figure S4). Sn²⁺ absorber contains large grains with some small grains at the bottom whereas Sn⁴⁺ absorber exhibits a clear double-layer structure with both layers consisting of well-packed large grains. In addition, ZnSe aggregates are observed on the surface of Sn²⁺ absorber from the SEM image (Figure 1f) whereas the surface of Sn⁴⁺ film is clean. We note that a tri-layer structure with a fine-grain middle layer is often observed for Sn⁴⁺ films (Figure S4b), which achieves similar efficiency as the double-layer film, whereas loosely packed small grains are frequently seen for Sn²⁺ films (Figure S4a). Further optimizing film fabrication condition to avoid the double-layer morphology is expected to further improve Sn⁴⁺ device performance. From the energy dispersive X-ray (EDX) spectroscopy measurement (Table S2), both Sn²⁺ and Sn⁴⁺ absorber films have a global Cu-poor and Zn-rich composition with Cu:Zn:Sn ratios of 1:0.71:0.62 for Sn²⁺ absorber and 1:0.71:0.65 for Sn⁴⁺ absorber. Compared to the feed-in composition (Cu:Zn:Sn=1:0.68:0.65), Sn²⁺ film exhibits slight Sn loss.

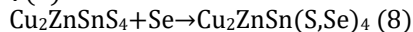
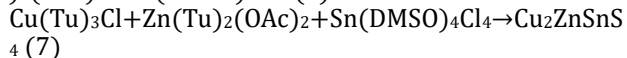
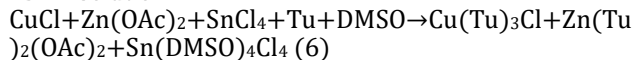
To understand the morphology and performance difference between Sn²⁺ and Sn⁴⁺ absorbers, solution chemistry) and reaction pathways from solution to absorber film were investigated (Figures S5 and S6). Solution chemistry shows that CuCl, ZnCl₂ and SnCl₂ coordinate with Tu and form Cu(Tu)₃Cl, Zn(Tu)₂Cl₂ and Sn(Tu)₂Cl₂, which respectively decomposes to Cu_{2-x}S, ZnS and SnS upon thermal annealing (Figure

S5). However, SnCl₄ only coordinates with DMSO and forms Sn(DMSO)₄Cl₄. Annealing a wet film containing SnCl₄ and Tu does not form SnS₂ due to direct decomposition of Sn(DMSO)₄Cl₄ to volatile SnCl₄ (boiling point 114.15°C). Investigation on the grain growth from precursor film to absorber material (Figure S7) reveals the amorphous CZTS in Sn²⁺ precursor film directly converted to CZTSSe by substitution reaction at the very early stage of selenization, whereas sulfides Cu_{2-x}S, ZnS and SnS in Sn²⁺ precursor film transferred to selenides Cu_{2-x}Se, ZnSe, and SnSe₂ first before converting to CZTSSe (more detailed grain growth mechanism of the two films will be reported in another paper). Thus, the reaction paths from Sn²⁺ and Sn⁴⁺ solutions to the CZTSSe absorbers can be written as follow:

Sn²⁺ solution:



Sn⁴⁺ solution:



Kim et al reported that the formation of defects is directly correlated to the existence of secondary phases and deep defects can be suppressed by reducing film inhomogeneity.[34] The co-existence of all three binaries in Sn²⁺ film during grain growth explains the poor uniformity and low device performance of Sn²⁺ absorber. On the contrast, the direct conversion of CZTS to CZTSe (Figure S7) enables compositional and morphological uniformity of Sn⁴⁺ absorber and thus superior device performance.

It has been reported that annealing kesterite absorber at low temperature for long time can reduce Cu-Zn disorder and improve absorber electronic property.[35] Recently, Yan et al. reported that heterojunction heat treatment (JHT) can reduce interface recombination and improve kesterite solar cell efficiency.[4] We had performed JHT of CdS/CZTSSe at 200°C for 20 h in vacuum. The J-V curves of Sn²⁺ and Sn⁴⁺ devices with and without JHT are shown in **Figure 2a** and their photovoltaic parameters are summarized in Table S3. For Sn²⁺ device, JHT only slightly increases V_{oc} but decreases J_{sc} and FF, resulting in slightly lower PCE. For Sn⁴⁺ device, on the contrary, JHT significantly improves V_{oc} and FF but slightly reduces J_{sc}. The best performing device with an active area efficiency of 13.0% (without ARC) was achieved from Sn⁴⁺ absorber with J_{sc} of 35.1 mA/cm², V_{oc} of 0.513 V, and FF of 72.5% (Figure 2a). The V_{oc,def} of this device is 0.317 V based on the bandgap of 1.070 eV extracted from the EQE (Figure S8). The statistical data of 20 h JHTed 150 devices (Figure S9 and Table S4, active area) show exactly the same trend as Figure 2a with the average J_{sc}, V_{oc}, FF and PCE of 34.7 mA/cm², 0.509 V, 70.7%, and 12.5% respec-

tively for Sn⁴⁺ devices, which again demonstrate the high reproducibility of Sn⁴⁺ absorber.

One of the 20 h JHTed high performance device with 98 nm MgF₂ ARC was independently measured by NREL and a total area efficiency of 11.56% with J_{sc} of 32.01 mA/cm², V_{oc} of 0.520 V and FF of 69.43% was certified on an area of 0.1066 cm² (Figure 2c and Figure S10c). The certified solar cell has an active area efficiency of 13.12% measured in house by excluding the grid area (Figure S10d). The J_{sc} integrated from the NREL measured EQE (Figure 2d) is 36.61 mA/cm², corresponding to an even higher active area efficiency of 13.22%. The V_{oc,def} of the certified device is 0.332 V based on the bandgap of 1.094 eV (Figure 2d), smaller than that of IBM (0.373V) and DGIST (0.345V) record devices.

From Yan et al, JHT leads to partial substitution of Zn by Cd which decreases absorber bandgap and increases device J_{sc}. [4] Su et al. also reported band gap decrease of kesterite with Cd alloying.[20] Glow discharge optical emission spectroscopy (GDOES, Figure 2e and 2f) shows both Sn²⁺ and Sn⁴⁺ absorber films have similar bulk compositional profiles with a large amount of Cd detected. However, the bandgap of our JHTed absorbers increases, from 1.041 to 1.065 eV for Sn²⁺ absorber and 1.050 to 1.070 eV for Sn⁴⁺ absorber, indicating different mechanism. Raman data (Figure 2g) clearly show a blue-shift of the CZTSSe peaks upon JHT, which is the direct evidence of improvement in kesterite disorder-order,[35] thus, the increase of the bandgap can be explained by the improvement in absorber order-disorder. To verify how much the order-disorder contributes to the V_{oc} enhancement, annealing absorber film without CdS was conducted under same condition (at 200°C for 20 h), which only improved device V_{oc} by 16 mV (Figure S11). The results indicate the order-disorder is not the vital issue for the large V_{oc,def} of kesterite solar cells, in agreement with Rey's report.[36]

The similar Cd diffusion, band gap increase and J_{sc} response of Sn²⁺ and Sn⁴⁺ absorbers upon JHT indicate JHT has similar effect on absorber bulk. The difference of JHT on device performance, that is, large improvement in V_{oc} and FF for Sn⁴⁺ device but slightly negative effect on Sn²⁺ device, has to come from the surface property of the absorber. From the reaction pathways discussed above, the uniform composition and direct conversion of kesterite phase of Sn⁴⁺ film ensures uniform composition and thus less defect surface. For Sn²⁺ film, on the contrary, the existence of multiphase until the end of the grain growth (Figure S8) inevitably creates high concentration of defects at the surface. To further confirm this, devices with different top and bottom precursor layers (top Sn⁴⁺/bottom Sn²⁺ or top Sn²⁺/bottom Sn⁴⁺) were fabricated and their J-V characteristics are shown in Figures 2h and 2i. As expected, the V_{oc} of devices with bottom Sn²⁺ and top Sn⁴⁺ layers gradually increase with the increase of Sn⁴⁺ layers and reaches that of pure Sn⁴⁺ device at 3 layers (Figure 2h and Table S5) whereas devices with bottom Sn⁴⁺ and top Sn²⁺ layers display linear decrease of V_{oc} with the increase of Sn²⁺ layers (Figure 2i and Table S6). In ad-

dition, devices with Sn⁴⁺ bottom layers have much higher FF than Sn²⁺ bottom layer devices, further confirming the high quality of the Sn⁴⁺ absorber materials. Further understand the mechanism of how JHT affects CZTSSe/CdS interface property of Sn⁴⁺ and Sn²⁺ based CZTSSe absorber is expected to provide more insight on the limiting factor of kesterite V_{oc}, which is under investigation and will be reported in the future.

The performance improvement of CZTS solar cell upon JHT was attributed to cation diffusion between CdS and CZTS and the JHT was conducted for a very short time.[4] We suspect the J_{sc} decrease in the 20 h JHTed devices comes from the deterioration of the absorber bulk property due to long time heat treatment at the presence of Cd. To confirm this, JHT of 2 h and 20 h were carried out on both Sn²⁺ and Sn⁴⁺ films and the results are shown in Figure S12 and Table S7. As expected, 2 h JHT resulted in better performance than 20 h JHT for both Sn²⁺ and Sn⁴⁺ devices with the main gain from J_{sc} for Sn²⁺ device and from both J_{sc} and FF for Sn⁴⁺ device. A champion device with a total area efficiency of 12.4% (no ARC) with J_{sc}, V_{oc}, FF of 33.32 mA/cm², 0.522 V and 71.5% was achieved from Sn⁴⁺ solution. The J-V and EQE characteristics of this device are shown in Figure 3. After excluding the grid area, this device has a J_{sc} of 36.36 mA/cm² (Figure 3a, dashed line), in excellent agreement with the J_{sc} (36.45 mA/cm²) integrated from the EQE, which corresponds to an active area efficiency of 13.6%. The band gap of this device extracted from the EQE is 1.058 eV. The V_{oc,def} and V_{oc}/V_{oc}^{SQ} of this device are calculated to be 0.297V and 63.7%, respectively. To our best knowledge, they are the lowest V_{oc,def} and highest V_{oc}/V_{oc}^{SQ} among all the reported kesterite solar cells.

CONCLUSIONS

In conclusion, we have used SnCl₄ and SnCl₂·2H₂O as tin precursor to investigate the effect of tin oxidation state on DMSO solution processed kesterite absorber property and solar cell performance. We found the coordination of Sn²⁺ with thiourea leads to a high crystalline precursor film containing SnS, ZnS and Cu_{2-x}S, whereas coordination of Sn⁴⁺ with DMSO results in direct formation of uniform amorphous kesterite phase. Although both precursor films converted to crystalline CZTSSe absorber upon selenization, Sn²⁺ film undergoes conversion of multiphase sulfides to selenides and then fusion of selenides to kesterite, resulting in poor absorber with non-uniform composition, on the contrast, direct conversion from sulfide to selenide kesterite ensures high quality absorber material of Sn⁴⁺ film. An active area efficiency of 12.2% with V_{oc} of 0.475 V was achieved from Sn⁴⁺ device which was only 8.84% with V_{oc} of 0.421 V for Sn²⁺ device. Furthermore, JHT greatly improves Sn⁴⁺ device performance but has slight negative effect on Sn²⁺ device. A champion device with a total area efficiency of 12.4% (without ARC), active area efficiency of 13.6%, lowest V_{oc,def} of 0.297 V, and highest V_{oc}/V_{oc}^{SQ} of 63.7% has been achieved from kesterite absorber fabricated from DMSO solution using Sn⁴⁺ precursor. Our results demonstrate a preformed uniform kesterite phase (as the Sn⁴⁺ precursor film in this report) is critical to en-

sure high quality absorber materials whereas fusion of multi secondary phases (as the Sn²⁺ precursor film in this report and most cases in the literature due to the starting precursors are metal or/and secondary sulfides) creates defects due to exist of secondary phases. Our finding provides a new platform and direction for investigating the mechanism of the V_{oc,def} issue of kesterite and further improving kesterite solar cell efficiency.

Received xxx 2020; accepted xxx 2020;
Published online xxx 2020

- 1 Todorov TK, Tang J, Bag S, *et al* Beyond 11% Efficiency: Characteristics of State-of-the-Art Cu₂ZnSn(S,Se)₍₄₎ Solar Cells. *Adv Energy Mater*, 2013, 3: 34-38
- 2 Xin H, Vorpahl SM, Collord AD, *et al* Lithium-doping inverts the nanoscale electric field at the grain boundaries in Cu₂ZnSn(S,Se)₍₄₎ and increases photovoltaic efficiency. *Phys Chem Chem Phys*, 2015, 17: 23859-23866
- 3 Qi Y-F, Kou D-X, Zhou W-H, *et al* Engineering of interface band bending and defects elimination via a Ag-graded active layer for efficient (Cu,Ag)₍₂₎ZnSn(S,Se)₍₄₎ solar cells. *Energy Environ Sci*, 2017, 10: 2401-2410
- 4 Yan C, Huang J, Sun K, *et al* Cu₂ZnSnS₄ solar cells with over 10% power conversion efficiency enabled by heterojunction heat treatment. *Nat Energy*, 2018, 3: 764-772
- 5 Guo L, Shi J, Yu Q, *et al* Coordination engineering of Cu-Zn-Sn-S aqueous precursor for efficient kesterite solar cells. *Sci Bull*, 2020, 65: 738-746
- 6 Giraldo S, Jehl Z, Placidi M, *et al* Progress and Perspectives of Thin Film Kesterite Photovoltaic Technology: A Critical Review. *Adv Mater*, 2019, 31: 1806692
- 7 Liu F, Wu S, Zhang Y, *et al* Advances in kesterite Cu₂ZnSn(S, Se)₄ solar cells. *Sci Bull*, 2020, 65: 698-701
- 8 Wang W, Winkler MT, Gunawan O, *et al* Device Characteristics of CZTSSe Thin-Film Solar Cells with 12.6% Efficiency. *Adv Energy Mater*, 2014, 4: 1301465
- 9 Son D-H, Kim S-H, Kim S-Y, *et al* Effect of solid-H₂S gas reactions on CZTSSe thin film growth and photovoltaic properties of a 12.62% efficiency device. *J Mater Chem A*, 2019, 7: 25279-25289
- 10 Nakamura M, Yamaguchi K, Kimoto Y, *et al* Cd-Free Cu(In,Ga)(Se,S)₍₂₎ Thin-Film Solar Cell With Record Efficiency of 23.35%. *IEEE J Photovolt*, 2019, 9: 1863-1867
- 11 Collord AD, Hillhouse HW. Germanium Alloyed Kesterite Solar Cells with Low Voltage Deficits. *Chem Mater*, 2016, 28: 2067-2073
- 12 Hadke S, Levchenko S, Sai Gautam G, *et al* Suppressed Deep Traps and Bandgap Fluctuations in Cu₂CdSnS₄ Solar Cells with ≈8% Efficiency. *Adv Energy Mater*, 2019, 9: 1902509
- 13 Chen S, Walsh A, Gong X-G, *et al* Classification of Lattice Defects in the Kesterite Cu₂ZnSnS₄ and Cu₂ZnSnSe₄ Earth-Abundant Solar Cell Absorbers. *Adv Mater*, 2013, 25: 1522-1539
- 14 Gunawan O, Todorov TK, Mitzi DB. Loss mechanisms in hydrazine-processed Cu₂ZnSn(Se,S)₄ solar cells. *Appl Phys Lett*, 2010, 97: 346-395
- 15 Min X, Guo L, Yu Q, *et al* Enhancing back interfacial contact by in-situ prepared MoO₃ thin layer for Cu₂ZnSnS₄Se_x solar cells. *Sci China Mater*, 2019, 62: 797-802
- 16 Kumar M, Dubey A, Adhikari N, *et al* Strategic review of secondary phases, defects and defect-complexes in kesterite CZTS-Se solar cells. *Energy Environ Sci*, 2015, 8: 3134-3159
- 17 Antunez PD, Bishop DM, Luo Y, *et al* Efficient kesterite solar cells with high open-circuit voltage for applications in powering distributed devices. *Nat Energy*, 2017, 2: 884-890
- 18 Siebentritt S. High voltage, please! *Nat Energy*, 2017, 2: 840-841
- 19 Haass SG, Andres C, Figi R, *et al* Complex Interplay between Absorber Composition and Alkali Doping in High-Efficiency Kesterite Solar Cells. *Adv Energy Mater*, 2018, 8: 1701760
- 20 Su Z, Tan JMR, Li X, *et al* Cation Substitution of

- Solution-Processed $\text{Cu}_2\text{ZnSnS}_4$ Thin Film Solar Cell with over 9% Efficiency. *Adv Energy Mater*, 2015, 5: 1500682
- 21 Girakdo S, Saucedo E, Neuschitzer M, *et al* How small amounts of Ge modify the formation pathways and crystallization of kesterites. *Energy Environ Sci*, 2018, 11: 582-593
- 22 Romanyuk YE, Haass SG, Girakdo S, *et al* Doping and alloying of kesterites. *J Phys Energy*, 2019, 1: 044004
- 23 Lee YS, Gershon T, Gunawan O, *et al* $\text{Cu}_2\text{ZnSnSe}_4$ Thin-Film Solar Cells by Thermal Co-evaporation with 11.6% Efficiency and Improved Minority Carrier Diffusion Length. *Adv Energy Mater*, 2015, 5: 1401372
- 24 Todorov T, Hillhouse HW, Aazou S, *et al* Solution-based synthesis of kesterite thin film semiconductors. *J Phys Energy*, 2020, 2: 012003
- 25 Xin H, Katahara JK, Braly IL, *et al* 8% Efficient $\text{Cu}_2\text{ZnSn}(\text{S},\text{Se})_4$ Solar Cells from Redox Equilibrated Simple Precursors in DMSO. *Adv Energy Mater*, 2014, 4: 1301823
- 26 Fu J, Fu J, Tian Q, *et al* Tuning the Se Content in $\text{Cu}_2\text{ZnSn}(\text{S},\text{Se})_4$ Absorber to Achieve 9.7% Solar Cell Efficiency from a Thiol/Amine-Based Solution Process. *ACS Appl Energy Mater*, 2018, 1: 594-601
- 27 Jiang JJ, Giridharagopal R, Jedlicka E, *et al* Highly efficient copper-rich chalcopyrite solar cells from DMF molecular solution. *Nano Energy*, 2020, 69: 11
- 28 Wu SP, Jiang JJ, Yu ST, *et al* Over 12% efficient low-bandgap $\text{CuIn}(\text{S},\text{Se})_2$ solar cells with the absorber processed from aqueous metal complexes solution in air. *Nano Energy*, 2019, 62: 818-822
- 29 Li J, Yuan Z-K, Chen S, *et al* Effective and Noneffective Recombination Center Defects in $\text{Cu}_2\text{ZnSnS}_4$: Significant Difference in Carrier Capture Cross Sections. *Chem Mater*, 2019, 31: 826-833
- 30 Kim S, Park J-S, Walsh A. Identification of Killer Defects in Kesterite Thin-Film Solar Cells. *ACS Energy Lett*, 2018, 3: 496-500
- 31 Ki W, Hillhouse HW. Earth-Abundant Element Photovoltaics Directly from Soluble Precursors with High Yield Using a Non-Toxic Solvent. *Adv Energy Mater*, 2011, 1: 732-735
- 32 Haass SG, Diethelm M, Werner M, *et al* 11.2% Efficient Solution Processed Kesterite Solar Cell with a Low Voltage Deficit. *Adv Energy Mater*, 2015, 5:
- 33 Gershon T, Shin B, Bojarczuk N, *et al* The Role of Sodium as a Surfactant and Suppressor of Non-Radiative Recombination at Internal Surfaces in $\text{Cu}_2\text{ZnSnS}_4$. *Adv Energy Mater*, 2015, 5: 1400849
- 34 Yang K-J, Sim J-H, Son D-H, *et al* Precursor designs for $\text{Cu}_2\text{ZnSn}(\text{S},\text{Se})_4$ thin-film solar cells. *Nano Energy*, 2017, 35: 52-61
- 35 Rey G, Redinger A, Sender J, *et al* The band gap of $\text{Cu}_2\text{ZnSnSe}_4$: Effect of order-disorder. *Appl Phys Lett*, 2014, 105: 112106
- 36 Rey G, Weiss TP, Sender J, *et al* Ordering kesterite improves solar cells: A low temperature post-deposition annealing study. *Sol Energy Mater Sol Cells*, 2016, 151: 131-138

Acknowledgements This work was supported primarily by the National Natural Science Foundation of China (NSFC, Grant No. 21571106, U1902218). Jiang J. and Yu S. acknowledge the support from Postgraduate Research and Practice Innovation Program of Jiangsu Province. Jedlicka E. and Giridharagopal R. acknowledge support of facilities in the Molecular Analysis Facility, a National Nanotechnology Coordinated Infrastructure site at the University of Washington which is supported in part by the National Science Foundation (grant NNCI-1542101), the University of Washington, the Molecular Engineering & Sciences Institute, the Clean Energy Institute, and the National Institutes of Health.

Author contributions Gong Y. and Xin H. conceived the idea and co-wrote the manuscript. Xin H. and Huang W. supervised the work. Gong Y. and Zhang Y. fabricated the devices and conducted most of the measurements. Jedlicka E. and Giridharagopal R. conducted GDOES measurements and initial data process. Clark J. conducted PL measurements. Niu C., Qiu R., Jiang J., Yu S. and Wu S. provides assistance in device fabrication and measurements. Yan W., Huang W., Hillhouse H. and Ginger D. discussed the results and provided valuable suggestions to the manuscript.

Conflict of interest The authors declare no conflict of interest.
Supplementary information Supporting data are available in the online version of the paper.

Figures:

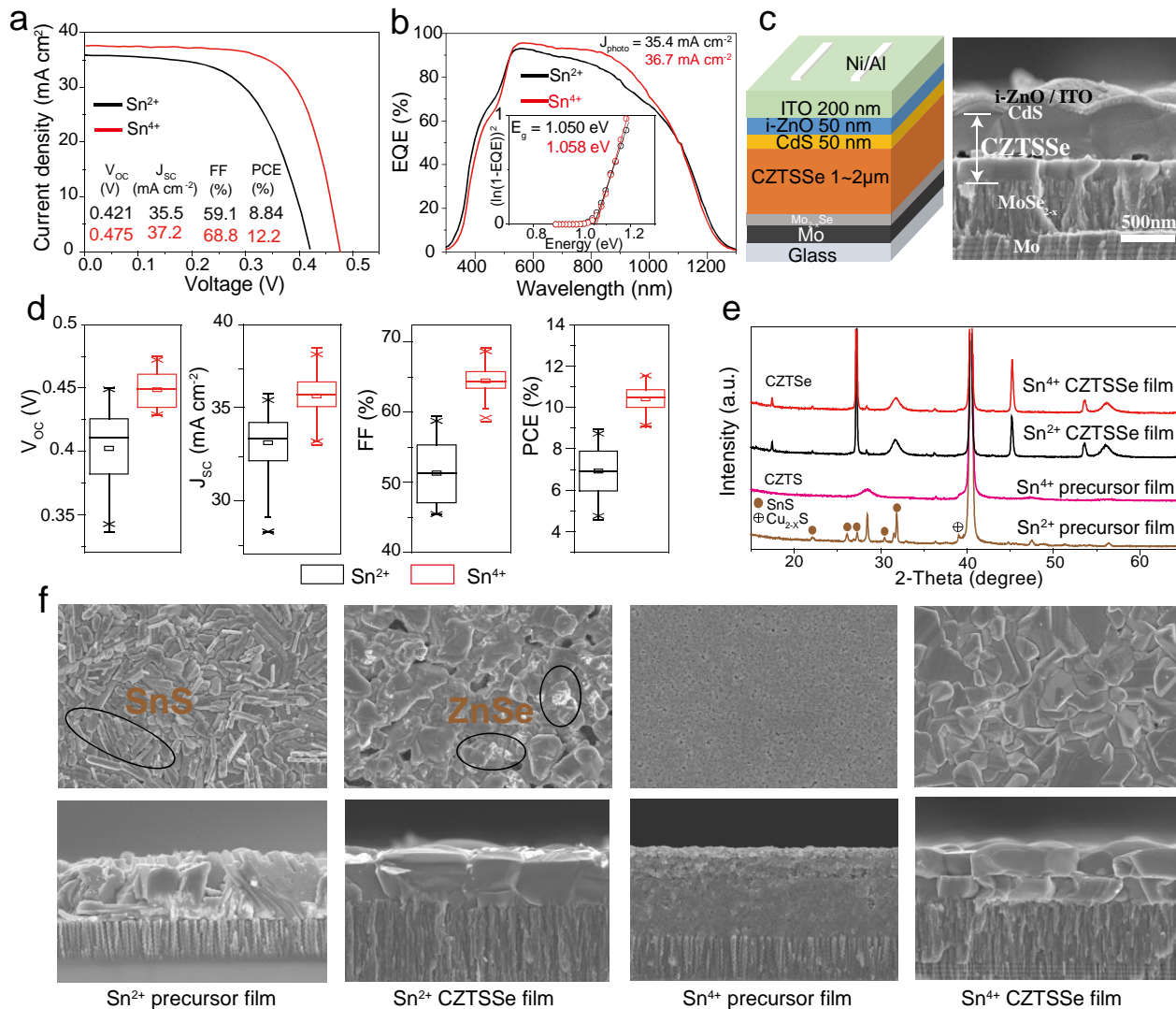


Figure 1. Characterization of CZTSSe devices and absorber films fabricated from Sn^{2+} and Sn^{4+} solutions. (a) J-V curves, (b) EQE spectra, (c) device structure, (d) statistical photovoltaic parameters, (e) XRD patterns, (f) plan view and cross-section SEM images of the precursor and absorber (CZTSSe) films. All images have the same scale. (b) Inset: Bandgap estimation by fitting the expected linear region of the EQE. Data in (d) are from 150 devices for each condition. Devices in (a) had 98 nm MgF_2 ARC. All efficiencies are based on active area.

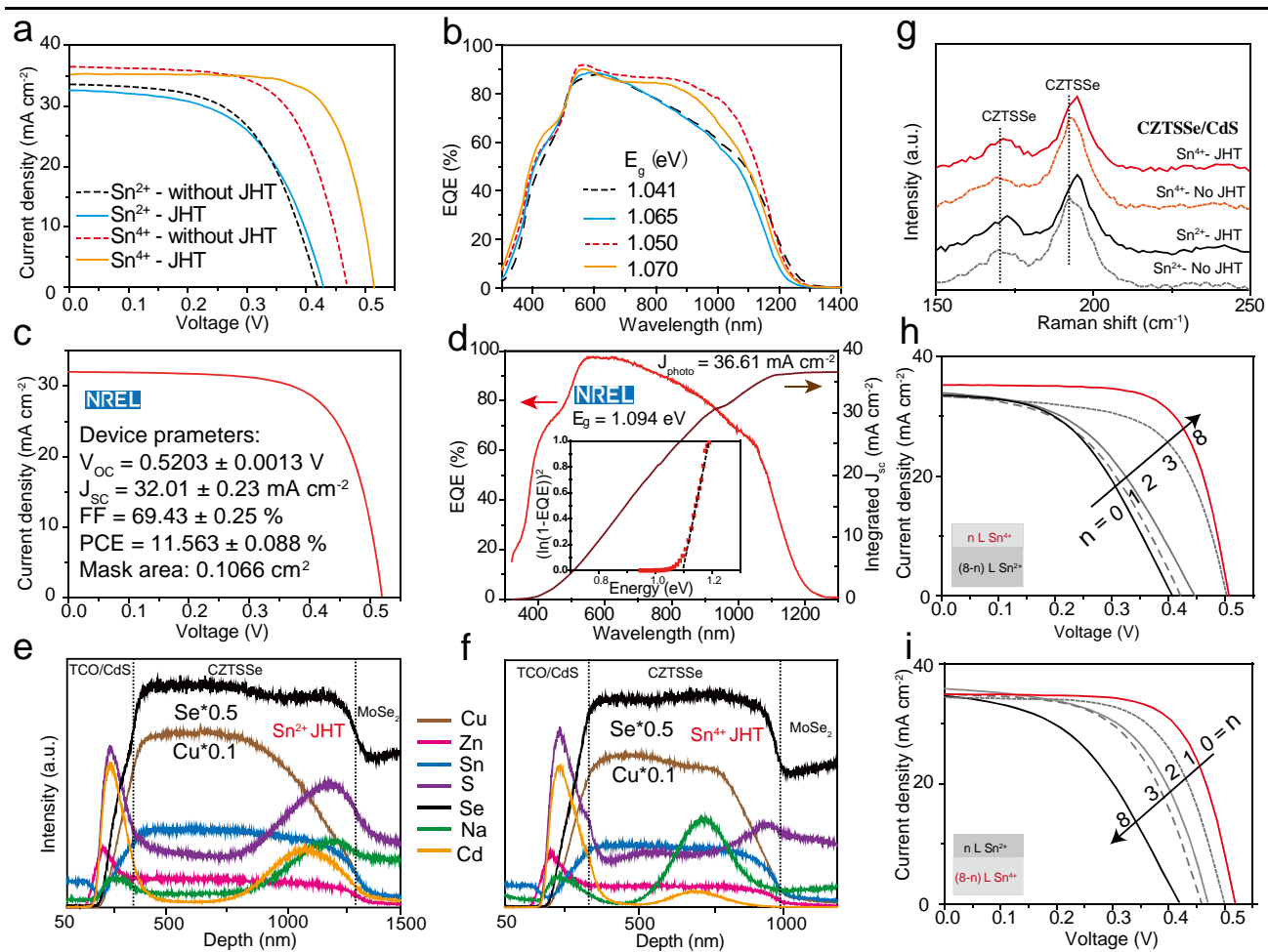


Figure 2. Effect of JHT on device performance. (a) J-V curves of Sn²⁺ and Sn⁴⁺ solar cells with and without JHT (no ARC); (b) EQE spectra of solar cells in (a); (c) The J-V and (d) the EQE of the NREL certified Sn⁴⁺ device; (e, f) Depth compositional profiles of JHTed Sn²⁺ (e) and Sn⁴⁺ (f) devices measured by GDOES; (g) Raman spectra of CdS/CZTSSe films with and without JHT (785 nm laser excitation); (h, i) J-V characteristics of devices with bottom Sn²⁺ and top Sn⁴⁺ layers (h) and bottom Sn⁴⁺ and top Sn²⁺ layers (i). The JHT was performed in vacuum for 20 h.

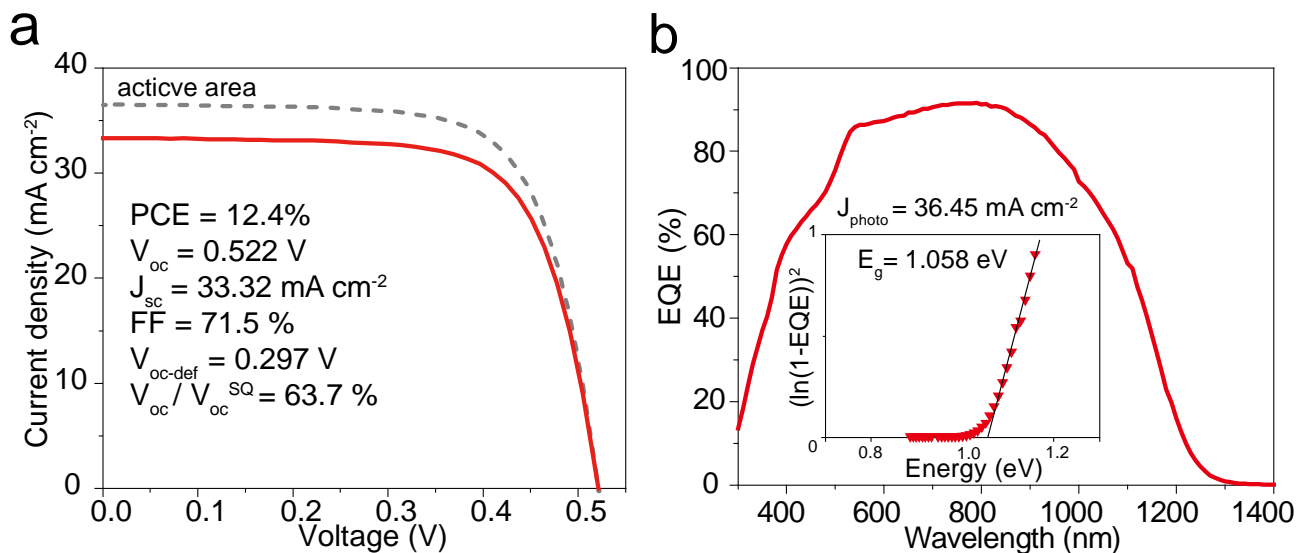


Figure 3. (a) J-V and (b) EQE of the champion CZTSSe device fabricated from Sn⁴⁺ precursor solution with 2h JHT.

Table of contents graphic

